ETH zürich

The role of magma mixing/mingling and cumulate melting in the Neapolitan Yellow Tuff caldera-forming eruption (Campi Flegrei, Southern Italy)

Journal Article

Author(s):
Forni, Francesca; Petricca, Eleonora; Bachmann, Olivier; Mollo, Silvio; De Astis, Gianfilippo; Piochi, Monica

ORIGINAL PAPER

The role of magma mixing/mingling and cumulate melting in the Neapolitan Yellow Tuff caldera-forming eruption (Campi Flegrei, Southern Italy)

Francesca Forni[1] · Eleonora Petricca[1] · Olivier Bachmann[1] · Silvio Mollo[2,3] · Gianfilippo De Astis[3] · Monica Piochi[4]

Abstract

Understanding the mechanisms responsible for the generation of chemical gradients in high-volume ignimbrites is key to retrieve information on the processes that control the maturation and eruption of large silicic magmatic reservoirs. Over the last 60 ky, two large ignimbrites showing remarkable zoning were emplaced during caldera-forming eruptions at Campi Flegrei (i.e., Campanian Ignimbrite, CI, ~ 39 ka and Neapolitan Yellow Tuff, NYT, ~ 15 ka). While the CI displays linear compositional, thermal and crystallinity gradients, the NYT is a more complex ignimbrite characterized by crystal-poor magmas ranging in composition from trachy-andesites to phonolites. By combining major and trace element compositions of matrix glasses and mineral phases from juvenile clasts located at different stratigraphic heights along the NYT pyroclastic sequence, we interpret such compositional gradients as the result of mixing/mingling between three different magmas: (1) a resident evolved magma showing geochemical characteristics of a melt extracted from a cumulate mush dominated by clinopyroxene, plagioclase and oxides with minor sanidine and biotite; (2) a hotter and more mafic magma from recharge providing high-An plagioclase and high-Mg clinopyroxene crystals and (3) a compositionally intermediate magma derived from remelting of low temperature mineral phases (i.e., sanidine and biotite) within the cumulate crystal mush. We suggest that the presence of a refractory crystal mush, as documented by the occurrence of abundant crystal clots containing clinopyroxene, plagioclase and oxides, is the main reason for the lack of erupted crystal-rich material in the NYT. A comparison between the NYT and the CI, characterized by both crystal-poor extracted melts and crystal-rich magmas representing remobilized portions of a "mature" (i.e., sanidine dominated) cumulate residue, allows evaluation of the capability of crystal mushes of becoming eruptible upon recharge.

Keywords Zoned ignimbrites · Caldera-forming eruption · Cumulate melting · Magma mixing · Neapolitan Yellow Tuff · Campi Flegrei

✉ Francesca Forni
 francesca.forni05@gmail.com

1 Institute of Geochemistry and Petrology, ETH Zürich, Clausiusstrasse 25, 8092 Zurich, Switzerland

2 Dipartimento di Scienze della Terra, Sapienza-Università di Roma, P.le Aldo Moro 5, 00185 Rome, Italy

3 Istituto Nazionale di Geofisica e Vulcanologia, via di Vigna Murata 605, 00143 Rome, Italy

4 Istituto Nazionale di Geofisica e Vulcanologia, Osservatorio Vesuviano, via Diocleziano 328, 80124 Naples, Italy

Introduction

The pyroclastic sequences deposited during large caldera-forming volcanic eruptions enclose crucial information about the mechanisms that govern the accumulation of large volumes of silicic magmas in the upper crust and the processes that lead to their explosive withdrawal (e.g., Smith and Bailey 1966; Lipman 1971; Blake 1981; Druitt and Bacon 1989; Wolff et al. 1990; de Silva 1991; Civetta et al. 1997). These pyroclastic sequences can display different styles of compositional zoning (see Hildreth 1981 and; Bachmann and Bergantz 2008 for reviews) which mirror a complex interplay between magma evolutionary processes (e.g., fractional crystallization, magma mixing, crustal

assimilation) and magma chamber dynamics (e.g., crystal settling, convection, melt extraction, reactive porous flow).

Over the last decades many authors have discussed the relative importance of fractional crystallization, crystal accumulation and melt extraction in generating chemical and physical gradients in upper crustal magma chambers (e.g., Lipman 1966; Wolff and Storey 1984; Worner and Schmincke 1984; Bacon and Druitt 1988; de Silva and Wolff 1995; Hildreth and Fierstein 2000; Hildreth and Wilson 2007). More recently, recharge events involving hotter and more mafic magmas of deeper origin have been suggested to play a key role in generating chemically zoned erupted sequences by partial melting of the crystalline material accumulated in the eruptible reservoir (i.e., cumulate mush; Kennedy and Stix 2007; Pamukcu et al. 2013; Bachmann et al. 2014; Wolff et al. 2015; Forni et al. 2016). Since the geochemical signatures of the processes that control the evolution of upper crustal reservoirs and eruption triggers are

often superimposed in the pyroclastic sequences, an accurate reconstruction of the pre-eruptive history of magma bodies can be extremely challenging. While bulk-rock geochemistry of juvenile clasts typically returns average compositions of various proportions of mineral phases and coexisting melts, detailed micro-analytical investigations of matrix glasses and mineral phases reveal much broader and complex compositional ranges. When combined with textural observations, these data can be extremely helpful in pinpointing the processes that control the accumulation, evolution and eruption of magmas associated with caldera collapses.

In this study we focus on the Neapolitan Yellow Tuff (NYT; 14.9 ka, Deino et al. 2004), an excellent example of complexly zoned ignimbrite erupted at Campi Flegrei during a cataclysmic caldera-forming event involving ~ 40 km^3 DRE (= dense rock equivalent) of alkaline magmas (Orsi et al. 1992, 1995; Scarpati et al. 1993) (Fig. 1). Complexly zoned pyroclastic sequences, such as the NYT, are not very
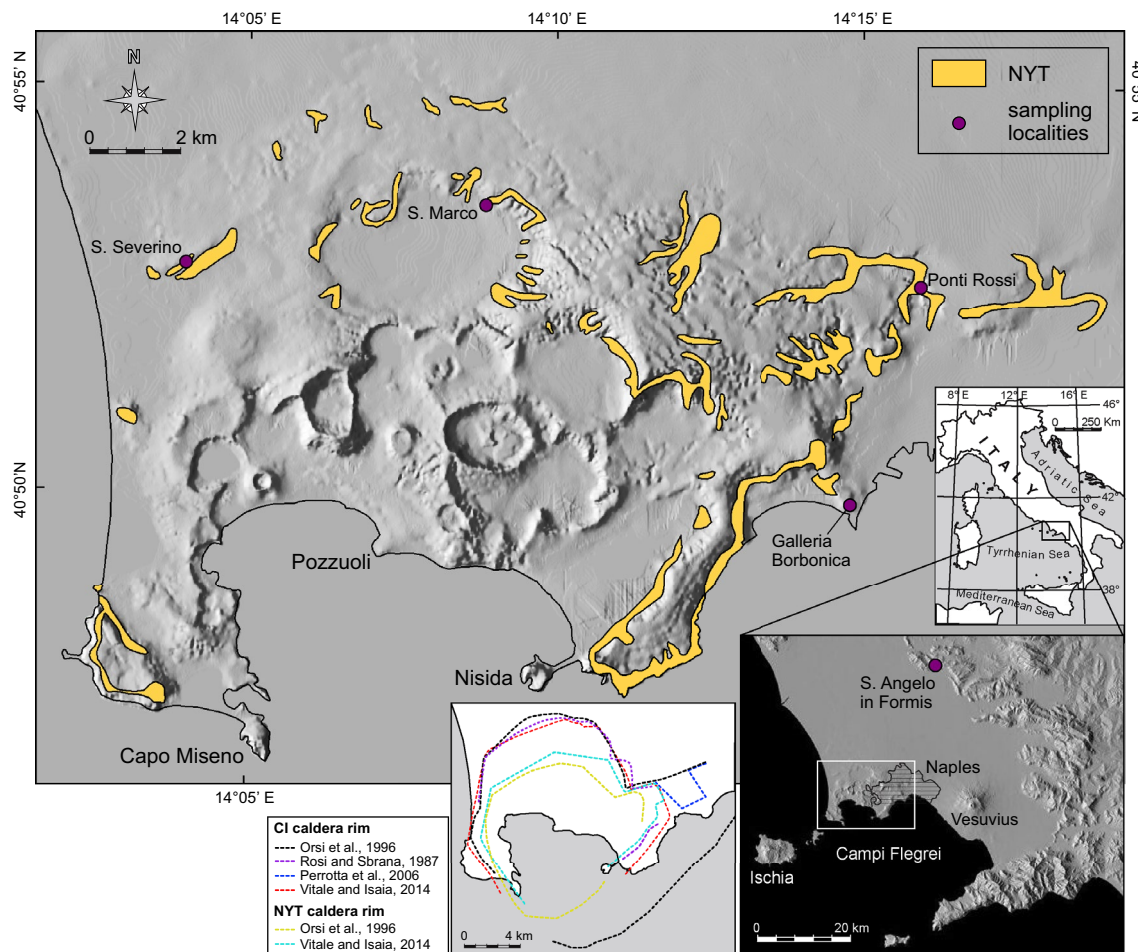
Fig. 1 Shaded relief map of the Campi Flegrei caldera showing the distribution of the NYT pyroclastic deposits (according to Pappalardo et al. 1999) and the sampling localities. In the insets: a simplified map of Italy and a shaded relief map of the Campanian Plain display-ing the location of the study area together with a simplified sketch of Campi Flegrei indicating the rims of the CI and the NYT calderas (colored dashed lines) according to the studies listed in the legend

common and have been interpreted as the result of either eruption of isolated magma domains which were stored and evolved in different conditions (e.g., Eichelberger et al. 2000; Shane et al. 2008; Ellis et al. 2014) or of a layered magma chamber which was tapped at different and fluctuating draw-down depths (e.g., Bacon and Druitt 1988; Orsi et al. 1995; Hildreth and Wilson 2007; Lipman et al. 2015). Differently from previous investigations mainly focused on bulk-rock geochemistry (Orsi et al. 1992, 1995; Scarpati et al. 1993), we report the results of a detailed micro-analytical study of mineral phases and matrix glasses from samples collected at different stratigraphic heights along the NYT pyroclastic sequence. We use our data to decipher the petrologic evolution of the NYT magmas and the dynamics of withdrawal. Finally, a comparison with the Campanian Ignimbrite (CI; ~ 39 ka, De Vivo et al. 2001) erupted during the first and largest caldera-forming event of Campi Flegrei (~ 200 km^3 DRE; Pappalardo et al. 2008) allows reconstruction of the architecture of the magmatic reservoirs that fed the two eruptions and provide new insights into crustal dynamics at active calderas.

The Neapolitan Yellow Tuff

The NYT pyroclastic sequence consists of two main units called Lower and Upper Member according to the nomenclature of Orsi et al. (1992, 1995) that is adopted in this study (Fig. 2) or, alternatively, Members A and B following Scarpati et al. (1993). The Lower Member consists of a sequence of pumice-and-ash fallout deposits and dilute pyroclastic density currents (PDCs) deposits which extend up to a distance of ~ 35 km from the vent and make ~ 1/3 of the total erupted volume (Orsi et al. 1992). The Upper Member comprises both massive and thick pumice-and-ash deposits from highly concentrated PDCs and stratified ash beds from dilute PDCs which were recognized up to a distance of ~ 14 km from the vent (Wohletz et al. 1995). A coarse lithic breccia corresponding to the onset of the caldera collapse phase was identified at the base of the Upper Member in the proximal areas (Scarpati et al. 1993). No paleosoils have been recognized between the two members in the field and $^{40}Ar/^{39}Ar$ dating confirms that the two units have the same age (14.9 ka; Deino et al. 2004). An angular unconformity and variations in the textural characteristics of the pyroclastic deposits were observed at the boundary between the two members. Such features were interpreted as the result of a change in the eruptive style from a central-vent phreato-plinian to a phreatomagmatic and magmatic phase related to multiple ring-fault vents associated with the caldera collapse (Orsi et al. 1995; Wohletz et al. 1995). Published bulk-rock and isotope data used to depict a well-defined chemostratigraphy indicate that the eruption was fed by a compositionally zoned reservoir hosting alkali-trachytic

to trachytic magmas and triggered by the arrival of a less evolved recharge magma (alkali-trachytic to latitic, showing slightly different Sr-isotope ratios; Orsi et al. 1995). The NYT deposits show lateral and vertical variations of the degree of lithification and zeolitization, which mostly depend upon the thermal conditions of deposition and the amount of phreatomagmatic water involved during eruption. The most lithified and zeolitized rocks are concentrated in the inner portions of the pyroclastic sequence in the proximal areas where the ignimbrite shows its maximum thickness. Here, relatively high temperatures (i.e., close to the water–vapor condensation) within the wet deposits were maintained long enough to trigger the hydration-dissolution processes in the volcanic glass (de'Gennaro et al. 2000).

Sampling and analytical methods

To investigate the geochemical variations in the NYT pyroclastic sequence, juvenile clasts were sampled at different stratigraphic heights in proximal and distal outcrops (Fig. 1). The sampled pyroclastic deposits from the Lower Member (LM) and Upper Member (UM) correspond to some of the stratigraphic units described by Orsi et al. (1992, 1995) (Fig. 2). Specifically, the Lower Member was sampled at S. Marco (LM1), Ponti Rossi (LM3) and S. Angelo in Formis (LM9, 11), whereas the Upper Member was sampled at S. Severino (UM1, 11, 13) and Ponti Rossi (UM16). Since sharp compositional variations were reported in the literature at the base of the Upper Member (Orsi et al. 1992, 1995), the unit UM1 was sampled at the bottom (UM1b) and at the top (UM1t) of the corresponding pyroclastic deposit. Additionally, pumiceous clasts from lithified facies were sampled at the same stratigraphic height from an underground tunnel underneath the city of Naples located at about 30 m below the ground level (Galleria Borbonica; GB2–4). According to the stratigraphic reconstructions reported in the Geological Map of Italy (ISPRA, Foglio 446–447 Napoli), pyroclastic deposits older than the Campanian Ignimbrite crop out in this area. Conversely, based on field observations and drill-hole data, Perrotta et al. (2006) indicate that in this area the NYT deposits extend from a depth of about 2–4 to 60–80 m below the ground level. This would imply that the sampled deposits are correlated with the NYT although their precise stratigraphic position in the pyroclastic sequence remains undefined.

Pumiceous clasts were powdered and analyzed for bulk-rock major and trace elements by XRF and ICPMS at ETH Zürich (see Online Resource 1 for a detailed description of the methods). Mineral phases and matrix glasses were separated, mounted in epoxy and analyzed for major and trace elements by EPMA and LA–ICPMS respectively at ETH Zürich. EPMA operative conditions were 15 kV acceleration voltage, counting times of 20 s on the peaks
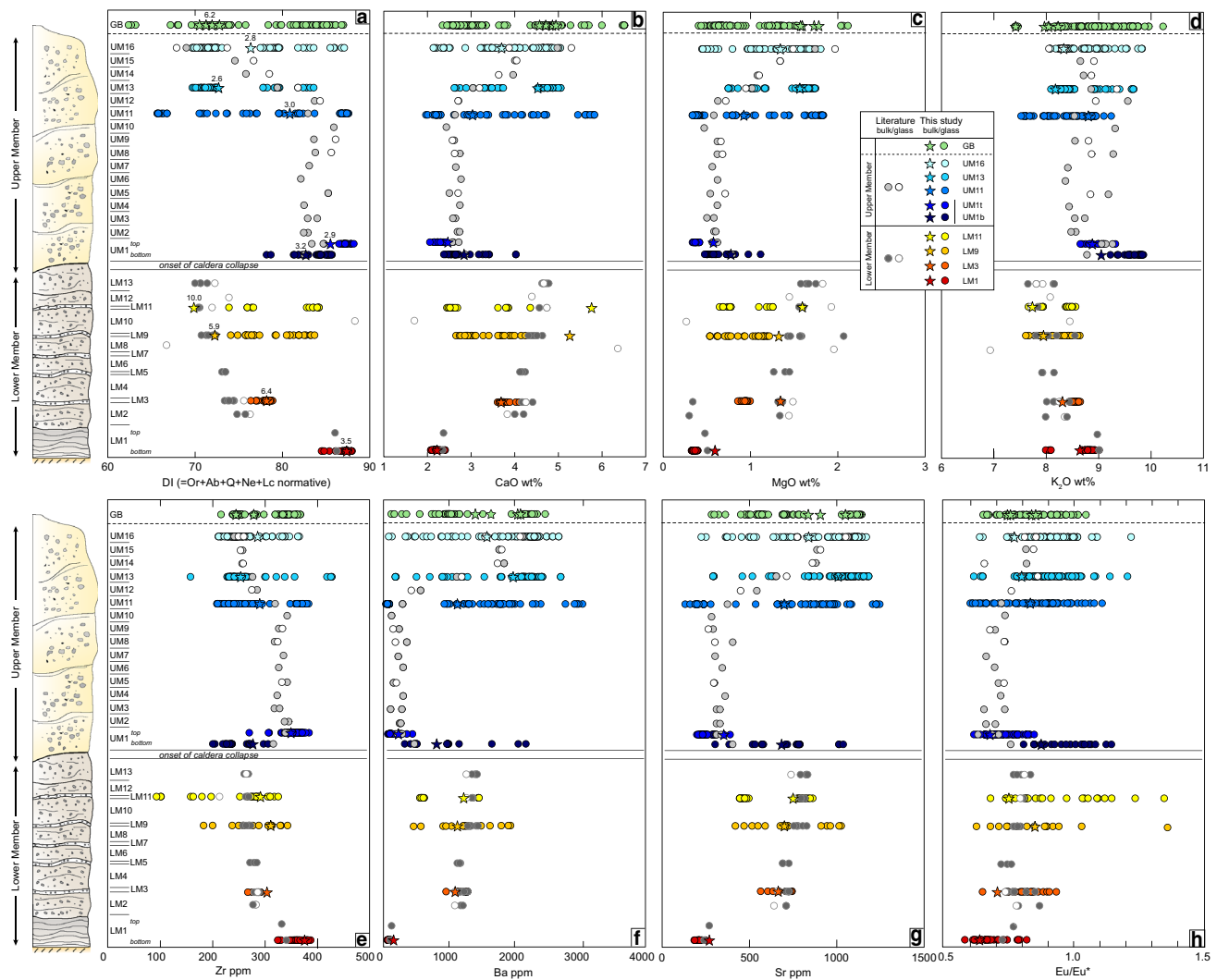
Fig. 2 Simplified section of the NYT pyroclastic sequence (after Orsi et al. 1992) and variation of geochemical parameters with stratigraphic height in the corresponding units: differentiation index (DI) (**a**); CaO (wt%) (**b**); MgO (wt%) (**c**); K$_2$O (wt%) (**d**); Zr (ppm) (**e**); Sr (ppm) (**f**); Ba (ppm) (**g**) and Eu/Eu* [=Eu$_N$/(Sm$_N$ × Gd$_N$)$^{1/2}$; trace element concentrations normalized to values from McDonough and Sun, 1995] (**h**). In **a** numbers denote the crystallinity of the corresponding samples. Grey symbols refer to data from the literature (Orsi et al. 1992, 1995; Scarpati et al. 1993; Wohletz et al. 1995) whereas colored symbols indicate data from this study.

Bulk-rock major element analyses are reported on anhydrous basis. Fe$_2$O$_3$ was converted to FeO (FeO = Fe$_2$O$_3$ × 0.8998) to compare bulk-rock data with the matrix glass compositions. DI is defined as Or + Ab + Q + Ne + Lc normative, according to Thornton and Tuttle (1960). Note that for the NYT normative quartz (Q) and leucite (Lc) are equal to zero. In the reconstructed stratigraphic section, LM1–13 correspond to the stratigraphic units distinguished by Orsi et al. (1992) for the Lower Member whereas UM1–16 have been renamed following the progressive order of samples from the base to the top of the Upper Member as reported in Orsi et al. (1992)

and 10 s on the backgrounds. The beam current was set at 20 nA for clinopyroxene and feldspar and decreased to 15 nA for biotite and glass analyses. To minimize alkali migration, a defocused beam was used for glass, feldspars and biotite analyses (20, 10, 5 µm, respectively), and K$_2$O and Na$_2$O were analyzed first. Analyses were typically reproducible to < 5% for all major oxides. LA-ICPMS is a 193 nm ArF Excimer laser from Resonetics coupled to a Thermo Element XR ICPMS. Spot sizes of 43 and 20 µm were used for mineral and glass analyses. The software

SILLS (Guillong et al. 2008) was used for data reduction using NIST612 and NIST610 as external standards and major element concentrations from EPMA as internal standards. The USGS reference glass GSD-1G was used as secondary standard to monitor the accuracy of the measurements. Repeat analyses (n = 53) of the USGS reference standard glass GSD-1G yielded external reproducibility (1SD) between 5 and 14%. The complete dataset of bulk-rock, mineral, matrix glass and standard compositions is reported in Online Resource 1.

For the isotopic analyses, bulk-rock powdered samples (~ 200 mg) from the base of the Lower and Upper Members (LM1 and UM1t) and from the Galleria Borbonica (GB2, GB3, GB4) were digested in HF and HNO_3 and diluted in HCl. Sr was separated by ion-exchange chromatography and samples were analyzed via thermal ionization mass spectrometry (TIMS) using a Thermo Scientific Triton-Plus mass spectrometer at ETH Zürich. Repeated $^{87}Sr/^{86}Sr$ measurements of the NBS 987 standard ($n = 8$) yielded the mean value of 0.710305 ± 0.000079 (2SD). The total procedure blanks (0.5 ng of Sr) were negligible for the analyzed samples.

Relative crystallinity was estimated by XRD using an AXS D8 Advance diffractometer equipped with a Lynxeye super speed detector at ETH Zürich following the method of Rowe et al. (2012). Powdered samples (< 20 μm) were analyzed using CuKα radiations generated at 40 kV and 40 mA. The following setting were used: 5°–90° (2θ scan interval), 0.02° (step size), 2 s (time/step), V12 (divergence and anti-scattering slits). Diffractograms were processed with the software OriginPro9, using the Peak Analyzer tool and Savitzky–Golay smoothing method. Integrated counts were calculated above the automatically determined linear background, giving the area of both amorphous and crystalline peaks (i.e., total area), and the cubic spline representing the area of crystalline peaks only (i.e., crystalline area). The relative crystallinity was calculated using the following formula: relative crystallinity (%) = (crystalline area/total area) × 100. All values were corrected according to a calibration curve obtained preparing powdered samples of known crystallinity by mixing various proportions of a granite (100% crystallinity) and amorphous glass (0% crystallinity). See Online Resource 1 for further information.

Results

Petrography, bulk-rock and matrix glass geochemistry

As a whole, the NYT pyroclastic rocks range in composition from trachy-andesites to phonolites ($SiO_2 = 55$–62 wt%; $Na_2O + K_2O = 11$–14 wt%; Online Resource 2) and contain between 3 and 10% crystals of sanidine, clinopyroxene, plagioclase, biotite, Ti-magnetite, and apatite. The matrix glass is unaltered and microlite-free, therefore, the measured crystallinity reflects the macrocrysts content. Crystal clots of mostly subhedral clinopyroxene, plagioclase, Ti-magnetite, apatite and rare biotite are abundant in the Upper Member (Online Resource 2). Binary plots of the differentiation index (DI) versus major elements show positive correlations with SiO_2, K_2O (Fig. 3a) and Na_2O (Fig. 3b) and negative correlations with MgO (Fig. 3c), CaO, TiO_2,

Fe_2O_3, P_2O_5, which indicate fractionation of clinopyroxene, biotite, Ti-magnetite, plagioclase and apatite. A decrease in K_2O and steeper increase in Na_2O at about DI ≥ 83 denote crystallization of sanidine (Fig. 3 a, b). Trace element variation diagrams display a steep decrease in Ba, Sr and Eu/Eu* with increasing Zr which indicates feldspar crystallization (Fig. 4a–c). Compared to the bulk-rock data, major and trace element compositions of matrix glasses reveal a much greater variability (Figs. 3, 4). Notably, some matrix glass compositions (e.g., LM9, LM11, UM1b and UM11) exhibit intermediate Sr and Ba, low Zr and slightly negative to positive Eu anomalies (Fig. 4a–c).

Chemostratigraphy

At the base of the Lower Member (LM1), bulk-rock and matrix glass compositions are homogeneously evolved (DI = 85–89) and display relatively low CaO, MgO, Ba and Sr contents together with high alkalis and Zr (Fig. 2). Above LM1, a sharp transition to less evolved compositions (DI = 71–78) showing higher CaO, MgO, Ba and Sr and lower Zr and alkalis is observed (LM2–3). Towards the top of the Lower Member, bulk-rock and matrix glasses span much broader compositional ranges (LM9, LM11, DI = 69–88) (Fig. 2). A compositional shift was detected at the base of the Upper Member with the occurrence of K_2O-Ba-Sr-rich compositions (UM1b, DI = 78–86) which become more evolved, homogenous and similar to LM1 towards the top of the same unit (UM1t, DI = 85–88) (Fig. 2). Extremely diverse compositions were found in the intermediate and top portions of the Upper Member (UM11, UM13, UM16, DI = 66–87). Compared to these units, the samples collected from the underground tunnel in Naples (Galleria Borbonica; GB2–4) show even wider compositional variations in bulk-rock and matrix glass geochemistry (DI = 63–87) (Fig. 2). Notably, matrix glass with positive Eu anomalies occurs in all the studied units except for LM1, LM3 and UM1t (Figs. 4f, 5h). Coherently with the remarkable geochemical heterogeneities observed in most of the analyzed units, mingling textures were identified in back-scattered images of dense glass fragments from the Upper Member and Galleria Borbonica (Online Resource 2). The crystallinity is slightly higher in the Lower Member (3.5–10% crystals) and in the samples from Galleria Borbonica (GB3; 6.2% crystals) compared to the Upper Member (2.6–3.2% crystals; Fig. 2a).

Sr-isotope geochemistry

To verify the stratigraphic position of the samples from Galleria Borbonica, bulk-rock Sr isotopic analyses were performed on all the samples collected in this location (GB2–4) and on two samples undoubtedly attributed to the
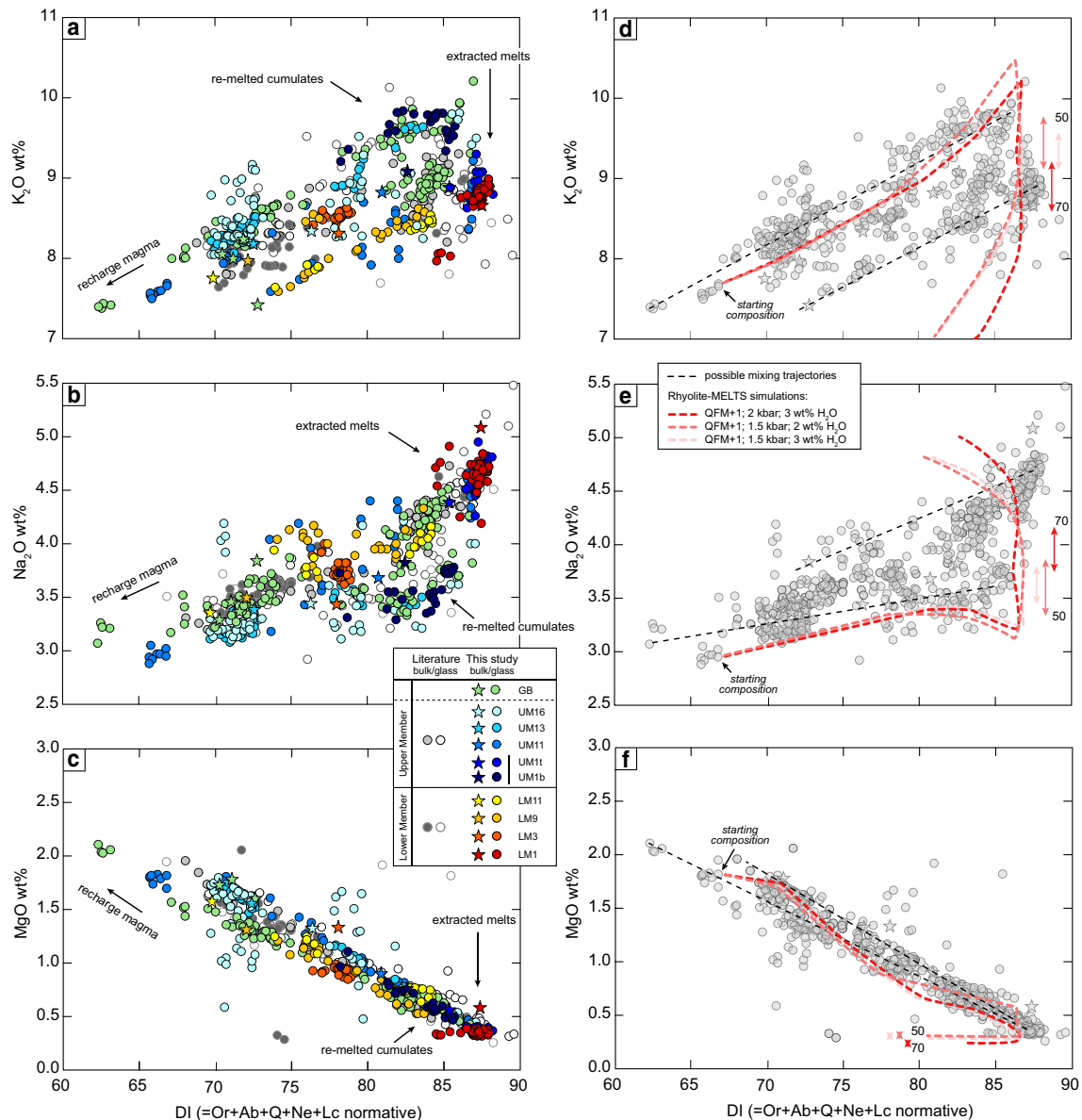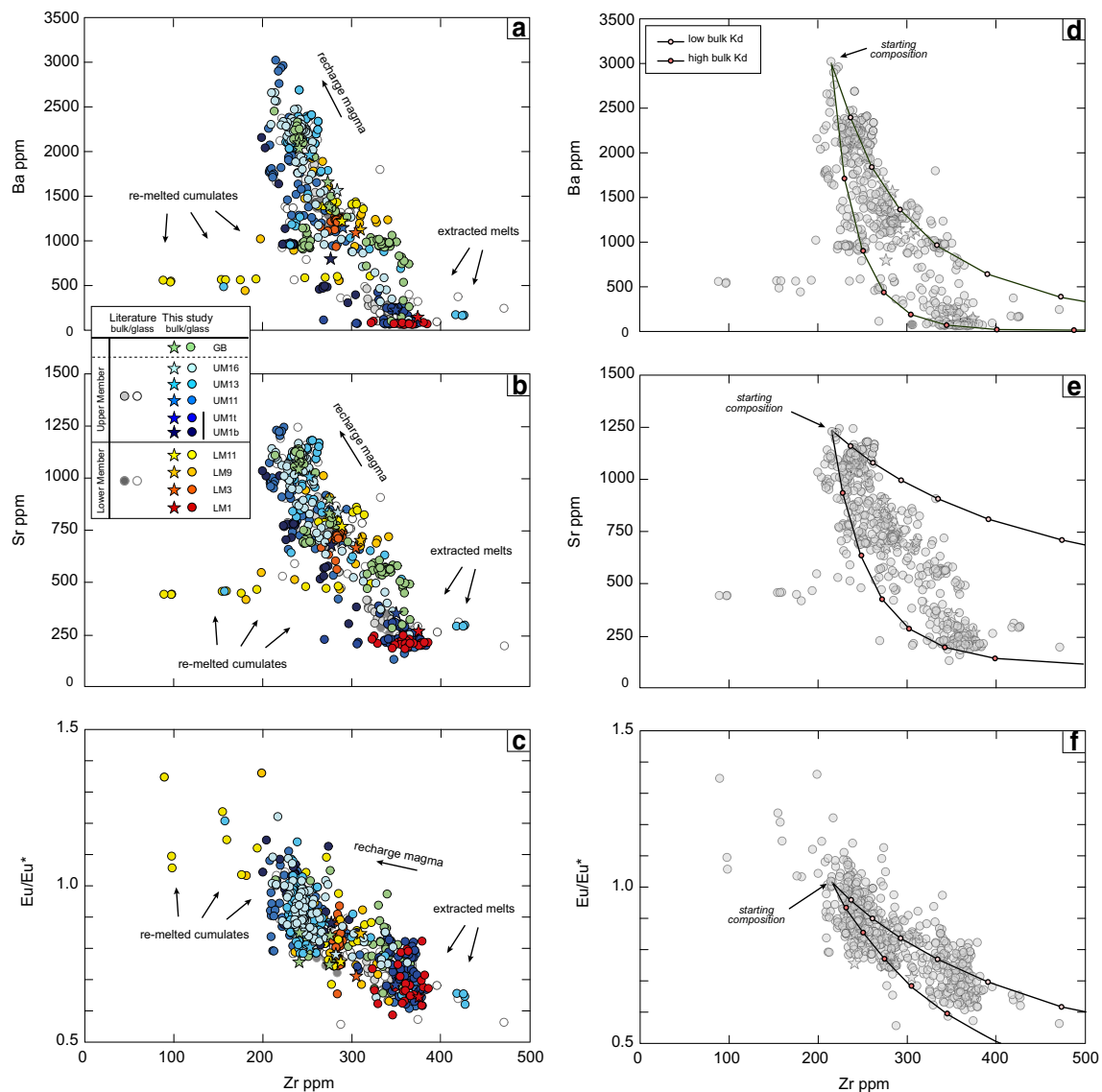
Fig. 3 Binary plots of differentiation index (DI) vs. K_2O (wt%) (**a**), Na_2O (wt%) (**b**) and MgO (wt%) (**c**) of bulk-rocks (color-filled symbols) and matrix glasses (white-filled symbols) from the NYT. Grey symbols refer to data from the literature (Orsi et al. 1992, 1995; Scarpati et al. 1993; Wohletz et al. 1995; Tomlinson et al. 2012), whereas colored symbols indicate data from this study. Bulk-rock major element analyses are reported on anhydrous basis. Fe_2O_3 was converted to FeO ($FeO = Fe_2O_3 \times 0.8998$) to compare bulk-rock data with the matrix glass compositions. DI is defined as $Or + Ab + Q + Ne + Lc$ normative, according to Thornton and Tuttle (1960). Note that for the NYT normative quartz (Q) and leucite (Lc) are equal to zero. For the same plots, crystallization paths (dashed colored lines) calculated using rhyolite-MELTS (Gualda et al. 2012) are reported in **d–f**. Vertical arrows indicate the crystallinity window suitable for melt extraction (50–70% crystals; Dufek and Bachmann 2010). Mixing lines connect the three magmatic components generating broad compositional ranges. See text and Online Resources 3 for further information

NYT pyroclastic sequence (LM1 and UM1t). The obtained isotopic ratios were compared with data from the literature referred to the entire range of volcanic activity at Campi Flegrei (literature data were normalized to the average value of NBS 987 standard measured in this study). The Sr isotopic ratios of the samples from Galleria Borbonica (GB2–4) vary between 0.70753 and 0.70755 (Fig. 5). These values are higher than those displayed by the pre-CI (0.70678–0.70746) and the CI samples (0.70732–0.70753) and partially overlap with the isotopic compositions of the post-CI/pre-NYT (0.70735–0.70764) and the post-NYT (0.70731–0.70871) eruptions (Fig. 5). The Sr isotopic signature of the GB2–4 samples closely overlap with the $^{87}Sr/^{86}Sr$ ranges reported in the literature for the NYT (0.70755–0.70761; Di Renzo

Fig. 4 Binary plots of and Zr (ppm) vs. Ba (ppm) (**a**), Sr (ppm) (**b**) and Eu/Eu* [=$Eu_N/(Sm_N \times Gd_N)^{1/2}$; trace element concentrations normalized to values from McDonough and Sun, 1995] (**c**) of bulk-rocks (color-filled symbols) and matrix glasses (white-filled symbols) from the NYT. Grey symbols refer to data from the literature (Orsi et al. 1992, 1995; Scarpati et al. 1993; Wohletz et al. 1995; Tomlinson et al. 2012) whereas colored symbols indicate data from this study. For the same plots, trace element fractional crystallization models obtained using the Rayleigh fractional crystallization equation for a range of bulk-rock partition coefficients, are reported in **d**–**f**. Symbols along the lines indicate melt fractions with steps of 0.1. See text and Online Resources 3 for further information

et al. 2011; Orsi et al. 1995) and those of the samples from the base of the Lower (LM1) and Upper (UM1t) Members analyzed in this study (0.70761 and 0.70756, respectively) (Fig. 5).

Chemistry and texture of mineral phases

Feldspars

Sanidine represents the most abundant mineral phase and is ubiquitous in the NYT juvenile clasts. Based on textural characteristics and compositional clustering, two main groups can be distinguished. Group 1 is more abundant and occurs in all the studied units, whereas group 2 is absent in LM1 and LM3 and is scarce in LM11 and UM1t (Fig. 6a). Group 1 (Or_{68-81}) is euhedral and weakly zoned in back-scattered images and display relatively low Ba and Sr contents (up to 6474 ppm and 3068 ppm, respectively; Fig. 6 b, c). Group 2 (Or_{79-89}) shows resorbed cores overgrown by bright rims, which reflect increasing Ba and Sr contents from core-to-rim (up to 25,517 and 3612 ppm, respectively; Fig. 6b, d).
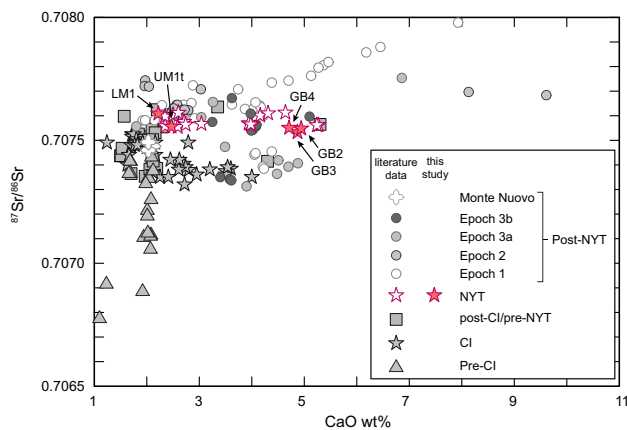
Fig. 5 Binary plot of bulk-rock CaO (wt%) vs. $^{87}Sr/^{86}Sr$ for different eruptions at Campi Flegrei. Grey symbols refer to Pre-CI, CI, post-CI/pre-NYT and post-NYT data from the literature (Civetta et al. 1997; D'Antonio et al. 1999, 2007; de Vita et al. 1999; Pappalardo et al. 1999, 2002, Pabst et al. 2008; Tonarini et al. 2009; Di Renzo et al. 2011; Di Vito et al. 2011). White-filled stars indicate NYT data from Scarpati et al. (1993), Orsi et al. (1995) and Di Renzo et al. (2011), whereas red-filled stars refer to NYT data from this study. Note that higher $^{87}Sr/^{86}Sr$ (up to 0.70871) and CaO (up to 10.7 wt%) compositions referred to the post-NYT activity, Epoch 1 (D'Antonio et al. 2007) are not represented in this plot. Literature data were normalized to the average value of NBS 987 standard measured in this study ($^{87}Sr/^{86}Sr = 0.710305$)

Plagioclase crystals are quite rare in the juvenile clasts of the NYT and range in composition from labradorite to anorthite (An_{51-93}; Online Resource 2). Labradoritic plagioclases (An_{63-51}) are euhedral and weakly zoned, with low-SrO contents (< 0.20 wt%; Online Resource 2). They were often recognized within crystal clots together with clinopyroxene, oxides and apatite (Online Resource 2). Bytownitic to anorthitic plagioclases (An_{68-93}) are only present in the Upper Member (UM13 and UM16) and samples from Galleria Borbonica (GB3 and GB4). They appear subhedral, sieve-textured and partially resorbed and have higher-Sr-Ba contents, often increasing towards more euhedral rims (Online Resource 2). Normally zoned crystals showing bytownitic cores and labradoritic rims were found in UM16, GB3 and GB4 (Online Resource 2).

Clinopyroxene

Euhedral clinopyroxene crystals ranging in composition from high-to-low-Mg diopside are widespread in NYT pyroclastic sequence. Three groups of clinopyroxene were recognized in the analyzed units (Fig. 7). Group 1 shows low-Mg clinopyroxenes (Mg# = 62–79) with variable Sr content (4–140 ppm) and negative Eu anomalies (Eu/Eu* = 0.3–0.8) (Fig. 7a–c). Group 1 crystals are poorly zoned and often form crystal clots together with labradoritic plagioclases, oxides and apatite (Fig. 7d; Online Resource 2). Group 2

includes high-Mg clinopyroxenes (Mg# = 77–93) with relatively high-Sr contents (56–126 ppm) and slightly negative Eu anomalies (Eu/Eu* = 0.6–0.9) (Fig. 7a–c). Group 2 crystals typically display high-Mg resorbed cores and rare preserved olivine crystals (Fo_{78}; Online Resource 2) overgrown by one or multiple intermediate-Mg zones and low-Mg thin bright rims, akin to group 1 clinopyroxene (Mg# = 66–73; Fig. 7 a, e). It is worth stressing that, although thin bright rims are ubiquitous in group 2 clinopyroxenes, only a few analyses are available due to the fact that in most cases the thickness of the crystal rims (1–2 microns) was smaller than the spot size of the electron microprobe and laser ablation. Group 3 clinopyroxenes were recognized in UM13 and in the samples from Galleria Borbonica (Fig. 7a). Compared with the other two groups, clinopyroxenes from group 3 show intermediate compositions (Mg# = 70–90) and significantly higher-Sr (84–250 ppm) and Eu/Eu* (0.7–1) (Fig. 7a–c). Most crystals are small (< 400 µ m) and appear poorly zoned in back-scattered images. Other crystals exhibit Mg-rich cores, akin to group 2 clinopyroxenes, overgrown by lower-Mg and higher-Sr-Eu/Eu* thick rims (Fig. 7f).

Other mineral phases

Euhedral biotite crystals (Mg# = 62–74) containing abundant melt, apatite and oxide inclusions are common in the NYT. Low-Sr–Ba–Co and high-Rb–Mn poorly zoned biotite crystals mainly occur in the most evolved and compositionally homogenous units (LM1 and UM1t), whereas relatively high-Co and low-Mn–Rb zoned crystals with increasing Sr and Ba from core-to-rim are common in all the other stratigraphic units (Online Resource 2). No correlation between Sr and Ba vs. Co and Mg# was observed in the zoned biotite crystals.

Ti-magnetite and apatite were recognized in all the analyzed units and often form crystal clots together with plagioclase and clinopyroxene (Online Resource 2) or occur as mineral inclusions in clinopyroxene and biotite. Relatively high TiO_2 and MnO magnetite crystals (Usp = 19–20) were found in most of the studied units, whereas relatively low TiO_2 and MnO magnetites (Usp = 14–18) showing negative correlation between Usp and V_2O_3 contents only occur in the Upper Member (UM1b and UM16) and in the samples from Galleria Borbonica (GB2 and GB4).

Intensive parameters

Equilibrium temperatures and magma water contents were obtained using clinopyroxene–liquid thermometers (Masotta et al. 2013) and K-feldspar-liquid hygrometers (Mollo et al. 2015) specifically calibrated to alkaline compositions, akin to the NYT magmas. Mineral cores and rims were combined with bulk-rock and matrix glass compositions,
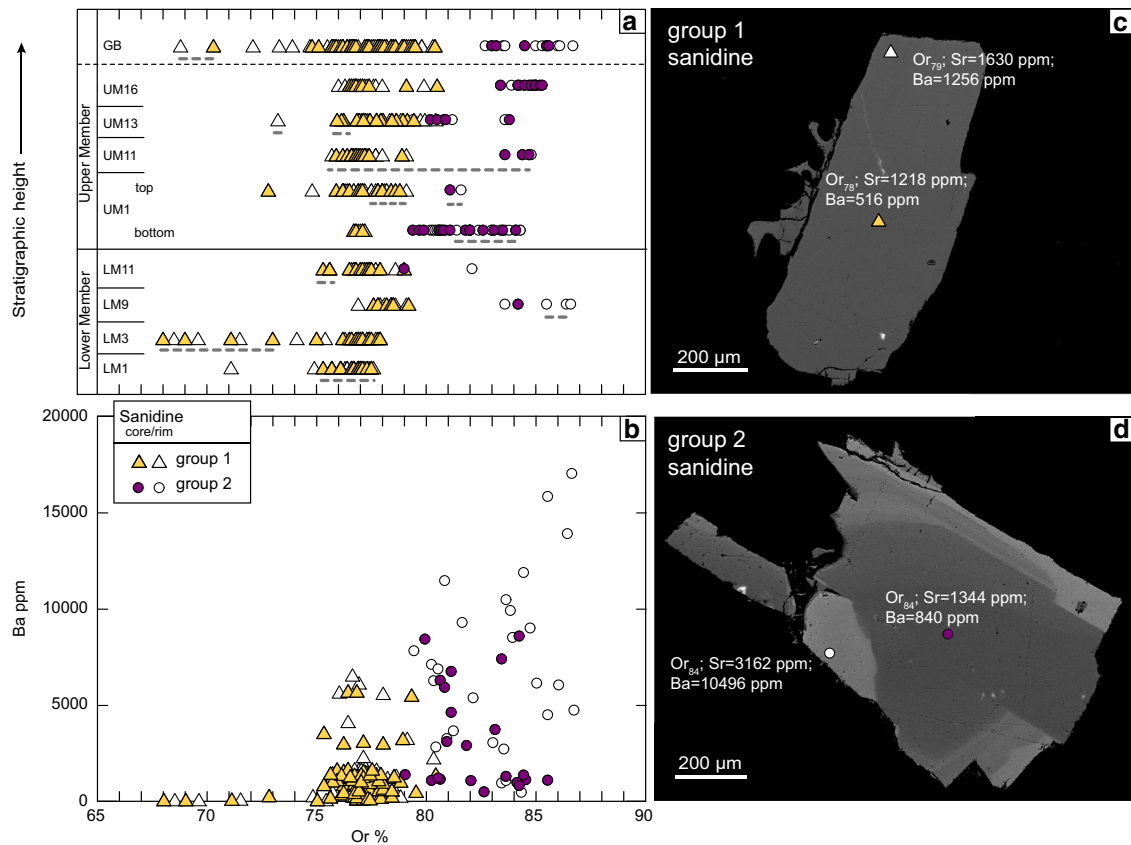
Fig. 6 Variation of Or% [= K/(Ca + Na + K) × 100] with stratigraphic height (**a**) and Ba (ppm) (**b**) in sanidine crystals from the NYT pyroclastic sequence showing distinction in two different groups. Backscattered image of group 1 unzoned sanidine (**c**) and group 2 sanidine displaying bright rims characterized by notable Sr and Ba enrichments (**d**). Grey dashed lines indicate the sanidine crystals that are out of equilibrium with the melt according to the equilibrium test of Mollo et al. (2015). See text for more details

respectively. Specifically, different populations of glass were distinguished for the units that show wide ranges of matrix glass compositions (LM9, LM11, UM11, 13, 16 and GB2–4). Mineral–liquid equilibria were tested using the methods described in Mollo and Masotta (2014) and Mollo et al. (2015) and only equilibrium pairs were used for the thermometric and hygrometric calculations. The standard errors of estimate associated with the clinopyroxene–liquid thermometer (± 18.2 °C) and K-feldspar–liquid hygrometer (± 0.7 wt%) are included in the intervals of temperature and water content reported below.

Relatively low temperatures and high-water contents were estimated for LM1 (~ 910–980 °C and ~ 4.1–6.2 wt%, respectively) and UM1t (~ 910–970 °C and ~ 4.2–6 wt%, respectively). Higher temperatures and slightly lower water contents were observed in LM3 (~ 980–1065 °C and ~ 4.6–4.9 wt%, respectively) and UMb (~ 940–1060 °C and ~ 4.2–5.9 wt%). Compared with these units much wider ranges of temperature and water contents were calculated for LM9, 11 and UM1b (~ 930–1060 °C and ~ 3.4–6.0 wt%, respectively), UM11, 13, 16 (920–1095 °C; 3.9–5.5 wt%,

respectively) and GB2–4 (930–1085 °C; 3.9–5.3 wt%). Equilibrium tests show that only group 1 clinopyroxene and sanidine are in equilibrium with LM1 and UM1t, whereas group 2 clinopyroxene (Mg# < 90) and group 1 sanidine (≥ Or$_{74}$) are in equilibrium with LM3 (Figs. 6a, 7a).

Discussion

Correlation between the pyroclastic deposits of Galleria Borbonica and the Neapolitan Yellow Tuff

The Sr isotopic ratios of the samples from Galleria Borbonica overlap with those of the NYT pyroclastic sequence and are clearly distinct from the Sr isotopic signatures of the pre-CI samples (Fig. 5). These findings suggest attribution of the deposits of Galleria Borbonica to the NYT pyroclastic sequence, thus confirming the stratigraphic reconstructions of Perrotta et al. (2006). We note that the samples GB2–4 bear remarkable geochemical and textural similarities with UM1b, UM11, UM13 and UM16:
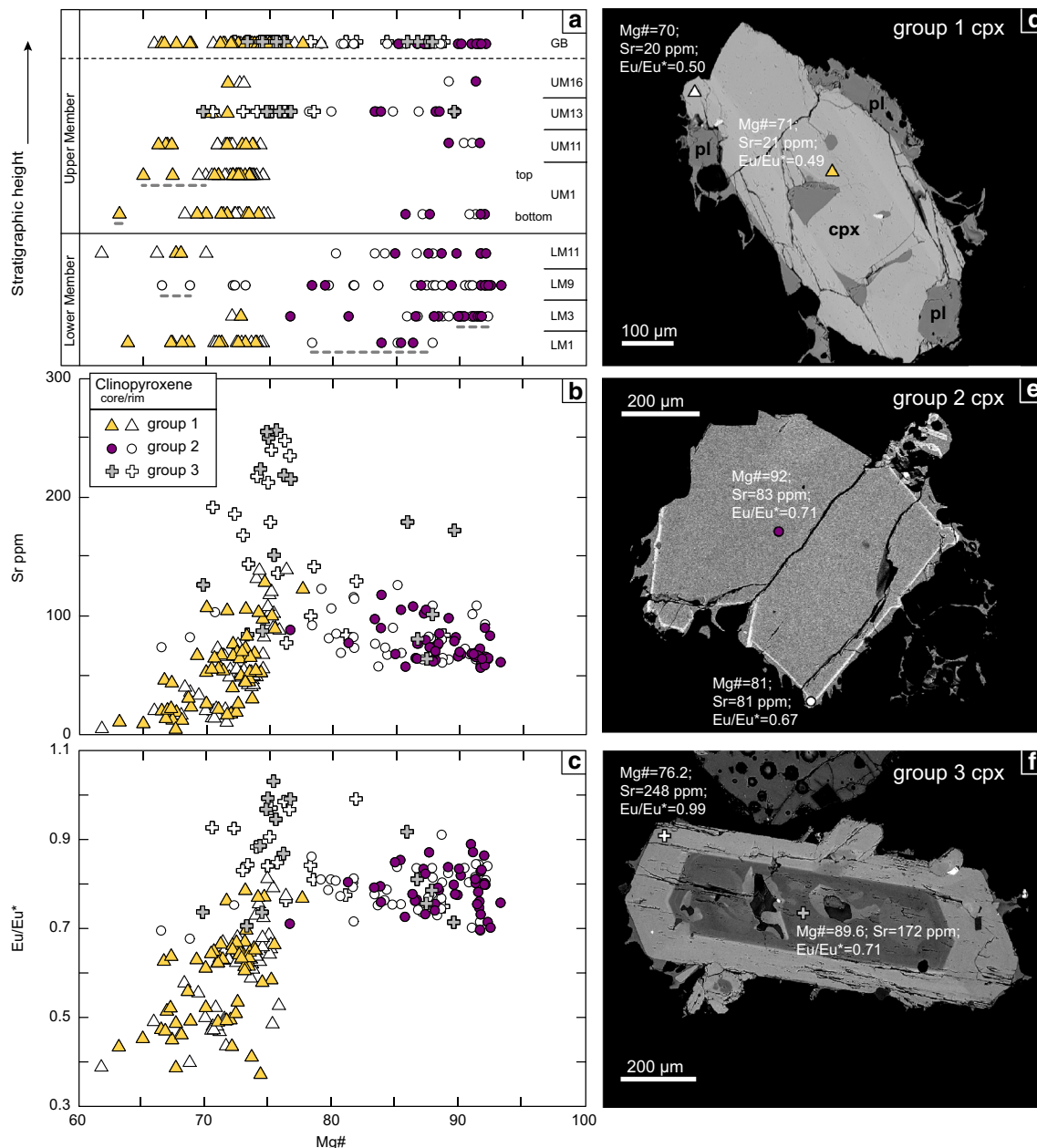
Fig. 7 Variation of Mg# [= Mg/(Mg + Fe) × 100] with stratigraphic height (**a**), Sr (ppm) (**b**) and Eu/Eu* [= $Eu_N/(Sm_N \times Gd_N)^{1/2}$; trace element concentrations normalized to values from McDonough and Sun, 1995] (**c**) in clinopyroxene crystals from the NYT pyroclastic sequence showing distinction in three different groups. Back-scattered image of poorly zoned group 1 clinopyroxenes with plagioclase crystals (**d**), group 2 clinopyroxenes displaying high-Mg cores and low-Mg bright rims (**e**) and group 3 clinopyroxenes showing high-Mg core and high-Sr-Eu/Eu* rims (**f**). Grey dashed lines indicate the clinopyroxene crystals that are out of equilibrium with the melt according to the equilibrium test of Mollo et al. (2013). See text for more details

(1) the broad compositional ranges observed in bulk-rock and matrix glasses (Figs. 2, 3, 4); (2) the mingling textures detected in back-scattered images of juvenile glass fragments (Online Resource 2); (3) the Sr enrichment in high-An plagioclases (Online Resource 2); (4) the occurrence of high-Sr-Eu clinopyroxenes (group 3; Fig. 7) and (5) the presence of relatively low-Ti–Mn magnetite crystals

(Online Resource 1). Hence, we propose a correlation between the pyroclastic deposits of Galleria Borbonica and the Upper Member of the NYT. Such correlation is further supported by the incipient lithification displayed by the pyroclastic deposits of Galleria Borbonica. Indeed, this post-depositional process typically affects the proximal

deposits in the intermediate and uppermost portions of the NYT pyroclastic sequence (de'Gennaro et al. 2000).

Role of fractional crystallization processes

The NYT is characterized by a wide range of compositions spanning from trachy-andesites to phonolites, and observable both at the scale of the entire pyroclastic sequence and within single juvenile clasts (Figs. 2, 3, 4). Despite such compositional variability, the Sr-isotope ratios show limited variations (i.e., 0.70753–0.70761; Di Renzo et al. 2011; Orsi et al. 1995; this study; Fig. 5) suggesting that the most evolved magmas may be genetically correlated with the least evolved ones. A slight decrease of the bulk-rock $^{86}Sr/^{87}Sr$ has been observed towards the top of the pyroclastic sequence indicating that a fresh and slightly less radiogenic recharge magma was injected at the base of the NYT magmatic reservoir prior or during eruption (Orsi et al. 1995). Rhyolite-MELTS (Gualda et al. 2012) thermodynamic simulations performed at different pressures and initial water contents (Fig. 3d–f) as well as fractional crystallization models obtained using a range of bulk-rock partition coefficients (see Online Resource 3 for further details) show that the least evolved compositions and the most differentiated ones plot on the same crystallization paths (i.e., liquid lines of descent; Fig. 4d–f). Additionally, mass balance calculations confirm that the highly evolved phonolitic compositions (LM1) can be derived from a trachy-andesitic parental magma akin to UM11 after ~60% fractional crystallization of sanidine (~28%), plagioclase (~16%), clinopyroxene (~8%), Ti-magnetite (~6%), biotite (~2%) and apatite (~1%) (Online Resource 3).

In agreement with experimental studies and thermodynamic calculations of trachy-phonolitic magmas at Campi Flegrei (Bohrson et al. 2006; Fowler et al. 2007; Fabbrizio and Carroll 2008), our rhyolite-MELTS simulations indicate that clinopyroxene is the liquidus phase followed by the late crystallization of feldspar (Online Resource 3). Consequently, in the early stages of magma cooling and differentiation, the geochemical evolution of clinopyroxene primary controls the concentration of rare earth elements (i.e., REE + Y where Y is a pseudo-lanthanide) in the solidifying system. This is especially true for Ce and Y that are highly incompatible in feldspar (i.e., $^{fsp-melt}D_{Ce}$ = 0.03 and $^{fsp-melt}D_{Y}$ = 0.07 from Mahood and Hildreth 1983 and; Ewart and Griffin 1994, respectively), but can be incorporated in clinopyroxene up to compatible trace element concentrations (Pappalardo et al. 2008). On this basis, the REE + Y model of Mollo et al. (2016) has been adopted to track the progressive variation of $^{cpx-melt}D_{Ce}$ and $^{cpx-melt}D_{Y}$ as a function of clinopyroxene compositional changes in the NYT (see Fig. 8 and Online Resource
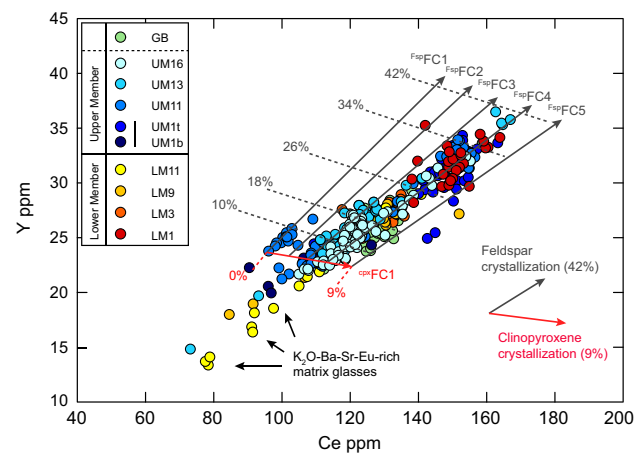
Fig. 8 Ce (ppm) vs. Y (ppm) diagram showing the geochemical evolution of the NYT products modelled using the Rayleigh fractional crystallization equation. At the beginning of the modelling, low degrees of clinopyroxene fractionation (i.e., 3, 5, 7, and 9%) have been considered. Stepwise calculations were performed changing the clinopyroxene composition and temperature at each step of fractionation. Modelled Ce and Y concentrations were used to draw the ^{cpx}FC vector. Fractional crystallization calculations were further developed accounting for the overall segregation of 42% of K-feldspar from the solidifying magma. Modelling results are aligned along five different trajectories from ^{kfs}FC1 to ^{kfs}FC5. Note that the matrix glasses from the K_2O–Sr–Ba-rich units displaying relatively low Ce and Y contents are not fully captured by the fractional crystallization model. See text and Online Resource 3 for more details

3 for the details of the model). Our fractional crystallization model shows that segregation of clinopyroxene (~9%) and feldspar (~42%), comparable with the results obtained via mass balance calculations (Online Resource 3), successfully reproduces the ranges of Ce and Y observed in the NYT. This confirms the development of a fractional crystallization-dominated environment prevalently controlled by the early formation of clinopyroxene at relative high temperature and the subsequent crystallization of variable amounts of feldspar during magma cooling. It is interesting to note that some compositions (e.g., LM9, LM11, UM1b, UM13) are not fully captured by the ^{cpx}FC1 and ^{fsp}FC1-5 vectors, as they are greatly depleted in Ce and Y (Fig. 8). Similarly, K_2O–Ba–Sr–Eu-rich and Zr-poor compositions referred to the same stratigraphic units, plot outside the main crystallization paths obtained by means of rhyolite-MELTS simulations (Fig. 3d–f) and trace element fractional crystallization models (Fig. 4d–f). These observations suggest that fractional crystallization alone cannot adequately account for the remarkable heterogeneity in melt and mineral compositions of the NYT magmas; some melting of feldspar and biotite-rich material must be taken into account (see discussion below).

Origin of textural and compositional variations

In a fractional crystallization-dominated environment crystal–liquid separation promotes the generation of a cumulate crystal mush, from which at intermediate crystallinity (~ 50–70% crystals; Dufek and Bachmann 2010) highly evolved interstitial melts can be extracted and accumulate in the upper portion of the eruptible reservoir (Bachmann and Bergantz 2004). Fractional crystallization and melt segregation processes undoubtedly played a key role in the evolution of the NYT magmas, producing the highly differentiated and water-rich compositions observed in LM1 and UM1t (Figs. 2, 3, 4). However, the remarkable heterogeneities displayed by the matrix glasses (Figs. 2, 3, 4, 8) and the presence of preserved mingling textures (Online Resource 2) indicate interactions between compositionally different magmas prior to eruption. Specifically, the occurrence of disequilibrium mineral phases in most of the studied units, even those that show relatively homogenous bulk-rock and matrix glass compositions (i.e., LM1, LM3 and UM1t; Figs. 6a, 7a), together with the presence of high-Mg clinopyroxene overgrown by low-Mg rims (group 2; Fig. 7), the resorbed bytownitic plagioclases overgrown by labradoritic rims (Online Resource 2) and the variations in Sr isotopic ratios, suggest interaction between a more mafic magma from recharge (showing slightly lower $^{87}Sr/^{86}Sr$) and the evolved resident melt. Additionally, the presence of matrix glass compositions (i.e., UM1b, LM11, UM11, UM13, UM16 and GB2–4) not captured by the fractional crystallization models (Figs. 3, 4, 8), indicate the occurrence of a third magmatic component. The geochemical characteristics of these matrix glasses suggest an origin via melting of K_2O–Ba–Sr–Eu-rich and N_2O–Zr–Ce–Y-poor mineral phases (i.e., feldspars ± biotite). This is further testified to by the occurrence of resorbed sanidines (group 2; Fig. 6), plagioclases and biotites (Online Resource 2) overgrown by Sr-Ba-rich rims and the high-Sr–Eu clinopyroxenes (group 3; Fig. 7) which record partial melting and re-crystallization from a locally enriched melt. Partial melting of feldspars and minor biotite could be likely triggered by the invasion of more mafic and hotter magma in the NYT magma chamber prior to eruption (see Wolff et al. 2015 for a review on this topic). Indeed, the notable temperature contrast between the most evolved compositions representing the resident magmas (~ 910 °C) and the least evolved ones indicative of the recharge magmas (up to ~ 1095 °C), is compatible with this scenario (see also the Bishop Tuff case, showing a similar thermal gradient, although the absolute temperatures are significantly lower; Evans et al. 2016 and references therein).

A comparison with the Campanian Ignimbrite

The CI and NYT caldera-forming eruptions display notable differences in the composition and crystallinity of erupted products (e.g., Orsi et al. 1995; Pappalardo et al. 2002, 2008; Thomlinson et al. 2012 and references therein). In the CI, crystal-poor evolved melts (5–6% crystals; DI = 86–91) fed most of the eruption until caldera collapse. Subsequently, crystal-rich and less differentiated magmas (36–37% crystals; DI = 75–78) were evacuated from the deeper and more crystalline portions of the sub-volcanic reservoir (Forni et al. 2016). The crystal-poor juvenile clasts display the geochemical features of melts extracted from a feldspar-dominated cumulate mush system (i.e., relatively high Zr, low-K_2O–Ba–Sr and negative Eu anomalies; Fig. 9a–c), whereas the crystal-rich juvenile material, erupted together with abundant alkali-syenites, exhibits a clear cumulate signature (i.e., relatively low Zr, high-K_2O–Ba–Sr and slightly negative to positive Eu anomalies; Fig. 9a–c).

In the NYT, only crystal-poor magmas showing a broad compositional range (3–10% crystals; DI = 72–87) were erupted. Evolved and relatively homogeneous products occur at the base and in the intermediate portions of the sequence, separated by more mafic and heterogeneous compositions, which become abundant towards the upper part of the ignimbrite (Fig. 2). We argue that the evolved magmas represent lenses of extracted melts showing limited interactions with the recharge magmas. Compared with the crystal-poor CI units, the NYT extracted melts display similar SiO_2, MgO and FeO contents but less pronounced Eu anomalies and higher CaO, K_2O, Sr and Ba contents, indicating lower degrees of feldspar fractionation (Fig. 9a–c). This is confirmed by results from mass balance calculations and trace element modeling showing that higher percentages of feldspar crystallization are required to derive the most evolved compositions of the CI (~ 64%; Pappalardo et al. 2008) compared with those of the NYT (~ 44%; see Fig. 8 and Online Resource 3).

Similarly to the CI, high-K_2O compositions displaying relatively high Zr, intermediate Ba and Sr contents and slightly negative to positive Eu anomalies occur in the NYT (Fig. 9a–c). Rhyolite-MELTS (Gualda et al. 2012) thermodynamic simulations and fractional crystallization models obtained for a range of input parameters and partition coefficients (see Online Resource 3) show that these compositions are not fully included in any of the possible crystallization paths of the CI and the NYT (Fig. 9d–f). Such behavior is coherent with an origin via melting of low temperature phases (i.e., sanidine ± biotite) in the cumulate mush upon more mafic recharge, which likely represents a key process in triggering both caldera-forming eruptions. In the CI evidence of the presence of a more mafic invading magma is given by the high-An plagioclase found in the crystal-rich
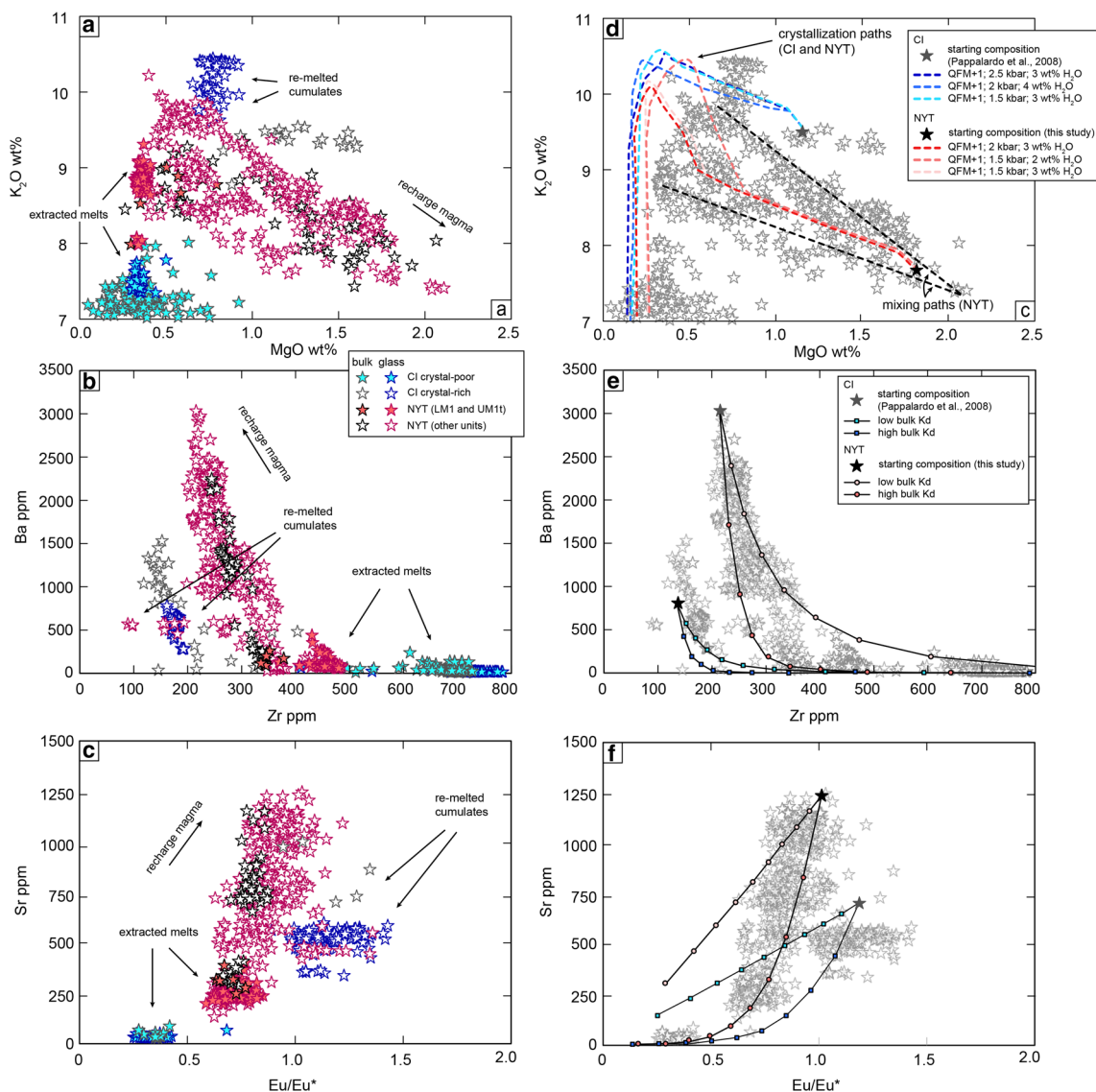
Fig. 9 Plot of MgO (wt%) vs. K$_2$O (wt%) (**a**), Zr (ppm) vs. Ba (ppm) (**b**) and Eu/Eu* [=Eu$_N$/(Sm$_N$ × Gd$_N$)$^{1/2}$; trace element concentrations normalized to values from McDonough and Sun, 1995] vs Sr (ppm) (**c**) in bulk-rock and matrix glasses from the CI and the NYT pyroclastic sequences. For the CI, compositions from the crystal-poor (color-filled symbols) and crystal-rich units (white-filled symbols) were distinguished (data from Melluso et al. 1995; Signorelli et al. 1999; Fedele et al. 2008; Forni et al 2016). For the NYT, compositions from the units LM1 and UM1t (color-filled symbols) and from all other units (white-filled symbols) were distinguished (data from Orsi et al. 1992, 1995; Wohletz et al. 1995; Tomlinson et al. 2012 and this study). Crystallization paths (dashed colored lines) calculated using rhyolite-MELTS (Gualda et al. 2012) are reported in **d**.

Trace elements fractional crystallization models obtained using the Rayleigh equation for a range of bulk-rock partition coefficients are reported in **e** and **f**. In **e** and **f** symbols along the lines indicate melt fractions with steps of 0.1. Note that both for the CI and the NYT the high-K$_2$O compositions showing low Zr, intermediate Ba and Sr and positive Eu anomalies are not included in the calculated crystallization paths, coherent with their origin via partial melting of low temperature phases in the cumulate mush. In the NYT, mixing lines connect the least evolved compositions (high-MgO–Sr–Ba and low-K$_2$O) with the remelted cumulates (high-K$_2$O and slightly negative to positive Eu anomalies) and the extracted melts (low-MgO–K$_2$O–Sr–Ba and negative Eu anomalies) generating broad compositional ranges. See text and Online Resources 3 for further information

portions but the compositional variations observed through the pyroclastic sequences (mainly due to strong changes in the crystallinity) indicate that small amounts of recharge magmas mixed with the resident evolved ones (Forni et al. 2016). Conversely, in the NYT, more pronounced interactions between the recharge magmas and the resident melts

are testified to by the presence of: (1) mingling textures and compositional heterogeneity in glass (Figs. 2, 3, 4 and Online Resource 2); (2) disequilibrium mineral phases (Figs. 6, 7); (3) notable scatter in major and trace element plots (Figs. 3, 4); (4) straight-line trajectories indicating magma mixing connecting the three different magmatic

components in major element diagrams (Figs. 2, 3, 9) and (5) slight decrease in $^{86}Sr/^{87}Sr$ towards the top of the pyroclastic sequence (Orsi et al. 1995).

Furthermore, in the NYT the occurrence of crystal clots notably lacking sanidine, suggests that K-feldspar was not abundant in the cumulate mush (Online Resource 2). Rhyolite-MELTS calculations confirm that in the NYT sanidine started crystallizing at a later crystallization stage compared to the CI (≥ 0.3 vs. ≥ 0.1 crystal volume fraction, respectively; see Online Resources 3). Hence, it is plausible that in the NYT sanidine was removed relatively late from the evolving magma depositing in the upper portion of the cumulate pile (group 2 sanidine) and continued crystallizing in equilibrium with the most differentiated melt without being removed from it (group 1 sanidine). Consequently, the bulk of the cumulate crystal mush was more refractory and more difficult to remobilize, thus explaining why, differently from the CI products, crystal-rich juvenile clasts were not found in the NYT pyroclastic sequence.

Dynamics of magma withdrawal

According to the reconstructions of Orsi et al. (1992) and Scarpati (1993), the NYT eruption started with a single conduit phreato-plinian phase during which the basal pumice layer LM1 was deposited. The geochemical characteristics of LM1 indicate that it represents portions of the evolved lens of extracted magma accumulated at the top of the eruptible reservoir, thus being the first to be erupted (Fig. 10a). In LM1, the occurrence of disequilibrium mineral phases (e.g., group 2 clinopyroxene; Fig. 7) suggests interaction with a less evolved recharging magma (Fig. 10b). When recharge entered the NYT magma chamber, convective stirring was activated due to thermal and physical perturbation promoting mixing between the invading and the resident magma. This is testified to by the presence of intermediate and relatively homogenous rock compositions (LM3; Fig. 10b) containing crystals from both the evolved and the more mafic magmas (i.e., low-Or sanidines and high-Mg clinopyroxene; Figs. 6, 7). As the eruption proceeded, deeper and more crystalline portions of the system became accessible, resulting in a slight increase of the crystallinity and compositional heterogeneity of the erupted magmas, as observed towards the upper portion of the Lower Member (LM9 and LM11) (Fig. 2). These magmas record mingling between the more mafic recharge and the high-K–Eu/Eu* magma derived from cumulate melting and become less crystalline and compositionally more homogeneous at the base of the Upper Member (UM1b). When the caldera collapse phase started, the opening of new fractures allowed tapping from other sectors of the eruptible reservoir where lenses of extracted melts were left almost undisturbed (Fig. 10c). This explains
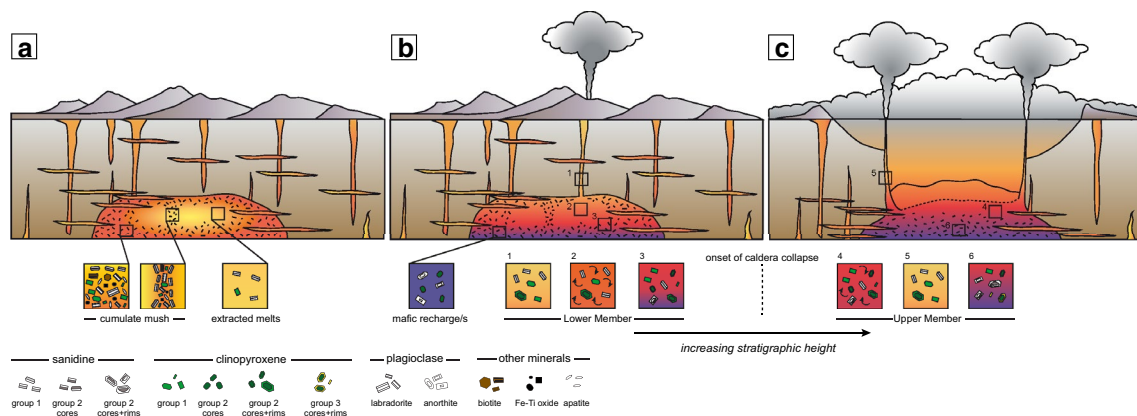
Fig. 10 Schematic cartoon illustrating the initial architecture of the NYT magmatic reservoir before eruption (**a**) and its subsequent evolution during eruption, as controlled by the dynamic of magma withdrawal (**b, c**). In **a** note the presence of a cumulate crystal mush dominated by group 1 clinopyroxenes, labradoritic plagioclases and oxides with minor biotite and sanidine crystals from which lenses of crystal-poor and relatively cold melts are extracted and accumulated in the upper part of the magmatic reservoir. In **b** more mafic magmas from recharge bring high-An plagioclases and high-Mg clinopyroxenes likely triggering the NYT eruption. The extracted melt ponding at the top of the magma reservoir is the first to be erupted (1). Note that despite the relatively homogeneous compositions of bulk-rocks and matrix glasses at the base of the Lower Member, the presence of disequilibrium high-Mg clinopyroxene cores overgrown by equilibrium low-Mg rims (group 2) testifies to interactions between the resident and the recharge magmas (1). Subsequently, mixing between these two magmas generates intermediate compositions (2). More heterogeneous compositions indicative of mingling between the recharge magma and a melt derived from melting of the low temperature phases within the cumulate mush (i.e., sanidine ± biotite) are present in the upper portion of the Lower Member (3) and become more homogenous in the lower part of the Upper Member (4). When caldera collapse occurs (**c**) eruption taps other sectors of the magma chamber where lenses of extracted melts are stored (5). Finally, mixing/mingling between all the different magmatic components generates the highly heterogeneous compositions, which occur at the top of the Upper Member (6)

the occurrence of evolved and homogeneous compositions akin to LM1 in the lower part of the Upper Member (UM1t) (Fig. 10c). Mixing/mingling between all the different components (i.e., evolved resident magma, magma derived from cumulate melting and more mafic magma from recharge) characterized the late phases of the eruption, producing the broad compositional ranges observed in the intermediate and upper portions of the Upper Member (UM11, UM13, UM16, GB2–4) (Figs. 2, 3, 4).

Conclusions

The Neapolitan Yellow Tuff (NYT) is a voluminous pyroclastic sequence erupted at ~15 ka during the most recent caldera-forming event of Campi Flegrei (Southern Italy). The compositional variations observed in the NYT do not reflect the inversion of a vertically zoned magma chamber but rather a complex interaction between different magmatic components stored in a heterogeneous upper crustal magma reservoir and progressively tapped (Orsi et al. 1992, 1995; this study). Indeed, the most evolved compositions (phonolites) occur at the base of the Lower and Upper Members and a sharp decrease in the degree of magma evolution (trachy-andesites) is observed towards the top of both units. By combining bulk-rock and glass geochemistry with textural and compositional features of mineral phases we show that at least three compositionally different magmas fed the NYT eruption: (1) an evolved magma displaying low-Ca–Mg–Ba–Sr and negative Eu anomalies; (2) a more mafic magma with high-Ca–Mg–Ba–Sr, low-K and slightly negative Eu anomalies and (3) an intermediate magma showing low-Ca–Mg, high-K, intermediate Ba and Sr and slightly negative to positive Eu anomalies. These three components variably interacted prior and during eruption generating the wide compositional ranges observed in the NYT bulk-rocks and matrix glasses. The geochemistry of the evolved products suggests that they represent the relatively cold and water-rich extracted melt accumulated in the upper part of the magmatic reservoir from which unzoned low-K–Sr–Ba sanidine (group 1), low-Mg clinopyroxene (group 1) and low-Sr–Ba–Co, high-Rb–Mn biotite crystallized. This magma fed the initial stages of eruption but was also erupted immediately after the caldera collapse, when new magma pathways opened, allowing tapping from different sectors of the reservoir. The relative more mafic component, showing slightly lower Sr-isotope ratios is representative of recharge magmas which mixed with the resident evolved melt as testified to by the presence of high-Mg clinopyroxene cores surrounded by thin bright low-Mg rims (group 2) and resorbed high-An plagioclase cores overgrown by lower-An rims. More mafic and hotter recharge triggered melting of the low temperature mineral phases (i.e., feldspars ± biotite)

accumulated in the upper part of the cumulate pile. These processes generated a compositionally intermediate melt enriched in K_2O, Ba, Sr and Eu from which high-Sr–Eu/Eu* clinopyroxene rims and crystals (group 3) together with high-Ba–Sr sanidine, plagioclase and biotite rims formed.

We conclude that the NYT represents a compelling example of pyroclastic sequence in which a combination of melt extraction, cumulate mush melting and mixing/mingling with recharge magmas play a key role in generating complex chemical and physical gradients. A similar scenario has been proposed for the CI (Forni et al. 2016) and other zoned ignimbrites around the world (e.g., Deering et al. 2011; Bachmann et al. 2014; Pamukcu et al. 2013; Wolff and Ramos 2014; Sliwinski et al. 2015, 2017; D'Oriano et al. 2017). However, differently from these other examples, erupted crystal-rich material with geochemical cumulate signature notably lacks in the NYT pyroclastic sequence (more akin to systems such as Yellowstone-Snake River Plain; e.g., Ellis et al. 2014). This implies that low temperature and highly fusible mineral phases (sanidine and biotite) did not represent the bulk of the cumulate mush system in the NYT magmatic reservoir. Hence, only detailed geochemical and textural analyses of matrix glasses and mineral phases allow reconstruction of the different processes that control the evolution of the upper crustal reservoir and those that lead to eruption.

References

Bachmann O, Bergantz GW (2004) On the origin of crystal-poor rhyolites: extracted from batholithic crystal mushes. J Petrol 45(8):1565–1582. https://doi.org/10.1093/Petrology/Egh019

Bachmann O, Bergantz GW (2008) Deciphering magma chamber dynamics from styles of compositional zoning in large silicic ash flow sheets. Rev Miner Geochem 69:651–674 doi: https://doi.org/10.2138/Rmg.2008.69.17

Bachmann O, Deering CD, Lipman PW, Plummer C (2014) Building zoned ignimbrites by recycling silicic cumulates: insight from the 1000 km(3) Carpenter Ridge Tuff, CO. Contrib Miner Petr 167(6) doi:https://doi.org/10.1007/S00410-014-1025-3

Bacon CR, Druitt TH (1988) Compositional evolution of the zoned calc-alkaline magma chamber of Mount Mazama, Crater Lake, Oregon. Contrib Miner Petr 98(2):224–256. https://doi.org/10.1007/BF00402114

Blake S (1981) Eruptions from zoned magma chambers. J Geol Soc 138(3):281–287. https://doi.org/10.1144/gsjgs.138.3.0281

Bohrson WA, Spera FJ, Fowler SJ, Belkin HE, De Vivo B, Rolandi G (2006) Petrogenesis of the Campanian Ignimbrite: implications for crystal-melt separation and open-system processes from major and trace elements and Th isotopic data. Volcanism in the Campania Plain: Vesuvius. Campi Flegrei Ignimbrites 9:249–288

Civetta L, Orsi G, Pappalardo L, Fisher RV, Heiken G, Ort M (1997) Geochemical zoning, mingling, eruptive dynamics and depositional processes—the Campanian Ignimbrite, Campi Flegrei caldera, Italy. J Volcanol Geotherm Res 75(3–4):183–219. https://doi.org/10.1016/S0377-0273(96)00027-3

D'Antonio M, Civetta L, Di Girolamo P (1999) Mantle source heterogeneity in the Campanian Region (South Italy) as inferred from geochemical and isotopic features of mafic volcanic rocks with shoshonitic affinity. Miner Petrol 67(3–4):163–192. https://doi.org/10.1007/Bf01161520

D'Antonio M, Tonarini S, Arienzo I, Civetta L, Di Renzo V (2007) Components and processes in the magma genesis of the Phlegrean Volcanic District, southern Italy. Geol Soc Am Spec Pap 418:203–220. https://doi.org/10.1130/2007.2418(10)

D'Oriano C, Landi P, Pimentel A, Zanon V (2017) Magmatic processes revealed by anorthoclase textures and trace element modeling: The case of the Lajes Ignimbrite eruption (Terceira Island, Azores). J Volcan Geotherm Res 347:44–63

de Silva SL (1991) Styles of zoning in central Andean ignimbrites; insights into magma chamber processes. Geol Soc Am Spec Pap 265:217–232. https://doi.org/10.1130/SPE265-p217

de Silva SL, Wolff JA (1995) Zoned magma chambers—the influence of magma chamber geometry on sidewall convective fractionation. J Volcanol Geotherm Res 65(1–2):111–118

de Vita S, Orsi G, Civetta L, Carandente A, D'Antonio M, Deino A, di Cesare T, Di Vito MA, Fisher RV, Isaia R, Marotta E, Necco A, Ort M, Pappalardo L, Piochi M, Southon J (1999) The Agnano–Monte Spina eruption (4100 years BP) in the restless Campi Flegrei caldera (Italy). J Volcanol Geotherm Res 91(2–4):269–301. https://doi.org/10.1016/S0377-0273(99)00039-6

De Vivo B, Rolandi G, Gans PB, Calvert A, Bohrson WA, Spera FJ, Belkin HE (2001) New constraints on the pyroclastic eruptive history of the Campanian volcanic Plain (Italy). Miner Petrol 73(1–3):47–65. https://doi.org/10.1007/S007100170010

de'Gennaro M, Cappelletti P, Langella A, Perrotta A, Scarpati C (2000) Genesis of zeolites in the Neapolitan Yellow Tuff: geological, volcanological and mineralogical evidence. Contrib Miner Petr 139(1):17–35. https://doi.org/10.1007/s004100050571

Deering CD, Bachmann O, Vogel TA (2011) The Ammonia Tanks Tuff: erupting a melt-rich rhyolite cap and its remobilized crystal cumulate. Earth Planet Sc Lett 310(3–4):518–525 doi. https://doi.org/10.1016/J.Epsl.2011.08.032

Deino AL, Orsi G, de Vita S, Piochi M (2004) The age of the Neapolitan Yellow Tuff caldera-forming eruption (Campi Flegrei caldera Italy) assessed by Ar-40/Ar-39 dating method. J Volcanol Geotherm Res 133(1–4):157–170. https://doi.org/10.1016/S0377-0273(03)00396-2

Di Renzo V, Arienzo I, Civetta L, D'Antonio M, Tonarini S, Di Vito MA, Orsi G (2011) The magmatic feeding system of the Campi Flegrei caldera: architecture and temporal evolution. Chem Geol 281(3–4):227–241. https://doi.org/10.1016/J.Chemgeo.2010.12.010

Di Vito MA, Arienzo I, Braia G, Civetta L, D'Antonio M, Di Renzo V, Orsi G (2011) The Averno 2 fissure eruption: a recent small-size explosive event at the Campi Flegrei Caldera (Italy). Bull Volcanol 73(3):295–320. https://doi.org/10.1007/s00445-010-0417-0

Druitt TH, Bacon CR (1989) Petrology of the zoned calcalkaline magma chamber of mount Mazama, Crater Lake, Oregon. Contrib Miner Petr 101(2):245–259. https://doi.org/10.1007/Bf00375310

Dufek J, Bachmann O (2010) Quantum magmatism: Magmatic compositional gaps generated by melt-crystal dynamics. Geology 38(8):687–690. https://doi.org/10.1130/G30831.1

Eichelberger JC, Chertkoff DG, Dreher ST, Nye CJ (2000) Magmas in collision: Rethinking chemical zonation in silicic magmas. Geology 28(7):603–606. https://doi.org/10.1130/0091-7613(2000)28<603:Micrcz>2.0.Co;2

Ellis BS, Bachmann O, Wolff JA (2014) Cumulate fragments in silicic ignimbrites: the case of the Snake River Plain. Geology 42(5):431–434. https://doi.org/10.1130/G35399.1

Evans BW, Hildreth W, Bachmann O, Scaillet B (2016) In defense of magnetite-ilmenite thermometry in the Bishop Tuff and its implication for gradients in silicic magma reservoirs. Am Miner 101(1–2):469–482

Ewart A, Griffin WL (1994) Application of proton-microprobe data to trace-element partitioning in volcanic-rocks. Chem Geol 117(1–2):251–284

Fabbrizio A, Carroll MR (2008) Experimental constraints on the differentiation process and pre-emptive conditions in the magmatic system of Phlegraean Fields (Naples, Italy). J Volcanol Geotherm Res 171(1–2):88–102. https://doi.org/10.1016/J.Jvolgeores.2007.11.002

Fedele L, Scarpati C, Lanphere M, Melluso L, Morra V, Perrotta A, Ricci G, 2008. The Breccia Museo formation, Campi Flegrei, Southern Italy: geochronology, chemostratigraphy and relationship with the Campanian Ignimbrite eruption. a 70:1189–1219

Forni F, Bachmann O, Mollo S, De Astis G, Gelman SE, Ellis BS (2016) The origin of a zoned ignimbrite: insights into the Campanian Ignimbrite magma chamber (Campi Flegrei, Italy). Earth Planet Sci Lett 449:259–271. https://doi.org/10.1016/j.epsl.2016.06.003

Fowler SJ, Spera F, Bohrson W, Belkin HE, De Vivo B (2007) Phase equilibria constraints on the chemical and physical evolution of the campanian ignimbrite. J Petrol 48(3):459–493. https://doi.org/10.1093/Petrology/Egl068

Gualda GAR, Ghiorso MS, Lemons RV, Carley TL (2012) Rhyolite-MELTS: a modified calibration of MELTS optimized for silica-rich, fluid-bearing magmatic systems. J Petrol 53:875–890

Guillong M, Meier DL, Allan MM, Heinrich CA, Yardley BWD (2008) SILLS: a MATLAB-based program for the reduction of laser ablation ICP-MS data of homogeneous materials and inclusions. Short Course Notes Geol Assoc Can 40:328–333

Hildreth W (1981) Gradients in silicic magma chambers—implications for lithospheric magmatism. J Geophys Res 86(Nb11):153–192. https://doi.org/10.1029/Jb086ib11p10153

Hildreth W, Fierstein J (2000) Katmai volcanic cluster and the great eruption of 1912. Geol Soc Am Bull 112(10):1594–1620. https://doi.org/10.1130/0016-7606(2000)112<1594:Kvcatg>2.0.Co;2

Hildreth W, Wilson CJN (2007) Compositional zoning of the Bishop Tuff. J Petrol 48(5):951–999. https://doi.org/10.1093/Petrology/Egm007

Kennedy B, Stix J (2007) Magmatic processes associated with caldera collapse at Ossipee ring dyke, New Hampshire. Geol Soc Am Bull 119(1–2):3–17. https://doi.org/10.1130/B25980.1

Lipman PW (1966) Water pressures during differentiation and crystallization of some ash-flow magmas from Southern Nevada. Am J Sci 264(10):810

Lipman PW (1971) Iron-titanium oxide phenocrysts in compositionally zoned ash-flow sheets from Southern Nevada. J Geol 79(4):438–456

Lipman PW, Zimmerer MJ, McIntosh WC (2015) An ignimbrite caldera from the bottom up: exhumed floor and fill of the resurgent Bonanza caldera, Southern Rocky Mountain volcanic field, Colorado. Geosphere 11(6):1902–1947. https://doi.org/10.1130/Ges01184.1

Mahood G, Hildreth W (1983) Large partition-coefficients for trace-elements in high-silica rhyolites. Geoch Cosmoch Acta 47(1):11–30

Masotta M, Mollo S, Freda C, Gaeta M, Moore G (2013) Clinopyroxene-liquid thermometers and barometers specific to alkaline differentiated magmas. Contrib Miner Petr 166(6):1545–1561. https://doi.org/10.1007/S00410-013-0927-9

McDonough WF, Sun SS (1995) The Composition of the Earth. Chem Geol 120(3–4):223–253. https://doi.org/10.1016/0009-2541(94)00140-4

Melluso L, Morra V, Perrotta A, Scarpati C, Adabbo M (1995) The eruption of the Breccia Museo (Campi-Flegrei, Italy)—fractional crystallization processes in a shallow, zoned magma chamber and implications for the eruptive dynamics. J Volcanol Geotherm Res 68:325–339

Mollo S, Masotta M (2014) Optimizing pre-eruptive temperature estimates in thermally and chemically zoned magma chambers. Chem Geol 368:97–103

Mollo S, Masotta M, Forni F, Bachmann O, De Astis G, Moore G, Scarlato P (2015) A K-feldspar-liquid hygrometer specific to alkaline differentiated magmas. Chem Geol 392:1–8. https://doi.org/10.1016/j.chemgeo.2014.11.010

Mollo S, Forni F, Bachmann O, Blundy JD, De Astis G, Scarlato P (2016) Trace element partitioning between clinopyroxene and trachy-phonolitic melts: a case study from the Campanian Ignimbrite (Campi Flegrei, Italy). Lithos 252–253:160–172 doi. https://doi.org/10.1016/j.lithos.2016.02.024

Orsi G, Dantonio M, Devita S, Gallo G (1992) The Neapolitan Yellow Tuff, a large-magnitude trachytic phreatoplinian eruption—eruptive dynamics, magma withdrawal and caldera collapse. J Volcanol Geotherm Res 53(1–4):275–287. https://doi.org/10.1016/0377-0273(92)90086-S

Orsi G, Civetta L, Dantonio M, Digirolamo P, Piochi M (1995) Step-filling and development of a 3-layer magma chamber—the Neapolitan-Yellow-Tuff case-history. J Volcanol Geotherm Res 67(4):291–312. doi:https://doi.org/10.1016/0377-0273(94)00119-2

Orsi G, DeVita S, diVito M (1996) The restless, resurgent Campi Flegrei nested caldera (Italy): constraints on its evolution and configuration. J Volcanol Geotherm Res 74(3–4):179–214. doi:https://doi.org/10.1016/S0377-0273(96)00063-7

Pabst S, Worner G, Civetta L, Tesoro R (2008) Magma chamber evolution prior to the Campanian Ignimbrite and Neapolitan Yellow Tuff eruptions (Campi Flegrei, Italy). Bull Volcanol 70(8):961–976. https://doi.org/10.1007/S00445-007-0180-Z

Pamukcu AS, Carley TL, Gualda GAR, Miller CF, Ferguson CA (2013) The evolution of the peach spring giant magma body: evidence from accessory mineral textures and compositions, bulk pumice and glass geochemistry, and rhyolite-MELTS modeling. J Petrol 54:1109–1148. https://doi.org/10.1093/petrology/egt007

Pappalardo L, Civetta L, D'Antonio M, Deino A, Di Vito M, Orsi G, Carandente A, de Vita S, Isaia R, Piochi M (1999) Chemical and Sr-isotopical evolution of the Phlegraean magmatic system before the Campanian Ignimbrite and the Neapolitan Yellow Tuff eruptions. J Volcanol Geotherm Res 91(2–4):141–166. https://doi.org/10.1016/S0377-0273(99)00033-5

Pappalardo L, Piochi M, D'Antonio M, Civetta L, Petrini R (2002) Evidence for multi-stage magmatic evolution during the past 60 kyr at Campi Flegrei (Italy) deduced from Sr, Nd and Pb isotope data. J Petrol 43(8):1415–1434. https://doi.org/10.1093/Petrology/43.8.1415

Pappalardo L, Ottolini L, Mastrolorenzo G (2008) The Campanian Ignimbrite (southern Italy) geochemical zoning: insight on the generation of a super-eruption from catastrophic differentiation and fast withdrawal. Contrib Miner Petr 156(1):1–26. https://doi.org/10.1007/S00410-007-0270-0

Perrotta A, Scarpati C, Luongo G, Morra V (2006) The Campi Flegrei caldera boundary in the city of Naples. Volcanism in the Campania Plain: Vesuvius. Campi Flegrei Ignimbrites 9:85–96

Rosi M, Sbrana A (1987) Phlegrean fields: petrography. Quad Ricerca Sci 114:60–79

Rowe MC, Ellis BS, Lindeberg A (2012) Quantifying crystallization and devitrification of rhyolites by means of X-ray diffraction and electron microprobe analysis. Am Miner 97(10):1685–1699 doi. https://doi.org/10.2138/am.2012.4006

Scarpati C, Cole P, Perrotta A (1993) The Neapolitan Yellow Tuff—a large-volume multiphase eruption from Campi Flegrei, Southern Italy. Bull Volcanol 55(5):343–356 doi. https://doi.org/10.1007/Bf00301145

Shane P, Smith VC, Nairn I (2008) Millennial timescale resolution of rhyolite magma recharge at Tarawera volcano: insights from quartz chemistry and melt inclusions. Contrib Miner Petr 156(3):397–411. https://doi.org/10.1007/S00410-008-0292-2

Signorelli S, Vaggelli G, Francalanci L, Rosi M (1999) Origin of magmas feeding the Plinian phase of the Campanian Ignimbrite eruption, Phlegrean Fields (Italy): constraints based on matrix-glass and glass-inclusion compositions. J Volcanol Geotherm Res 91:199–220

Sliwinski JT, Bachmann O, Ellis BS, Dávila-Harris P, Nelson BK, Dufek J (2015) Eruption of shallow crystal cumulates during explosive phonolitic eruptions on Tenerife, Canary Islands. J Petrol 56(11):2173–2194. https://doi.org/10.1093/petrology/egv068

Sliwinski JT, Bachmann O, Dungan MA, Huber C, Deering CD, Lipman PW, Martin LHJ, Liebske C (2017) Rapid pre-eruptive thermal rejuvenation in a large silicic magma body: the case of the Masonic Park Tuff, Southern Rocky Mountain volcanic field, CO, USA. Contrib Miner Petr 172(5):30. https://doi.org/10.1007/s00410-017-1351-3

Smith RL, Bailey RA (1966) The Bandelier Tuff: a study of ash-flow eruption cycles from zoned Magma Chambers. Bull Volcanol 29(1):83–103. https://doi.org/10.1007/BF02597146

Thornton CP, Tuttle OF (1960) Chemistry of igneousrocks.1. Differentiation Index. Am J Sci 258(9):664–684

Tomlinson EL, Arienzo I, Civetta L, Wulf S, Smith VC, Hardiman M, Lane CS, Carandente A, Orsi G, Rosi M, Muller W, Menzies MA (2012) Geochemistry of the Phlegraean Fields (Italy) proximal sources for major Mediterranean tephras: Implications for the dispersal of Plinian and co-ignimbritic components of explosive eruptions. Geochim Cosmochim Ac 93:102–128. https://doi.org/10.1016/j.gca.2012.05.043

Tonarini S, D'Antonio M, Di Vito MA, Orsi G, Carandente A (2009) Geochemical and B-Sr-Nd isotopic evidence for mingling and mixing processes in the magmatic system that fed the Astroni volcano (4.1–3.8 ka) within the Campi Flegrei caldera (southern Italy). Lithos 107(3–4):135–151 doi. https://doi.org/10.1016/J.Lithos.2008.09.012

Vitale S, Isaia R (2014) Fractures and faults in volcanic rocks (Campi Flegrei, southern Italy): insight into volcano-tectonic processes. Int J Earth Sci (Geol Rundsch) 103(3):801–819. https://doi.org/10.1007/s00531-013-0979-0

Wohletz K, Orsi G, Devita S (1995) Eruptive Mechanisms of the Neapolitan-Yellow-Tuff Interpreted from stratigraphic, chemical, and granulometric data. J Volcanol Geotherm Res 67(4):263–290. https://doi.org/10.1016/0377-0273(95)00002-C

Wolff JA, Ramos FC (2014) Processes in Caldera-forming high-silica rhyolite magma: Rb–Sr and Pb isotope Systematics of the Otowi Member of the Bandelier Tuff, Valles Caldera, New Mexico, USA. J Petrol 55(2):345–375. https://doi.org/10.1093/petrology/egt070

Wolff JA, Storey M (1984) Zoning in highly alkaline magma bodies. Geol Mag 121(6):563–575

Wolff JA, Worner G, Blake S (1990) Gradients in physical parameters in zoned felsic magma bodies—implications for evolution and

eruptive withdrawal. J Volcanol Geotherm Res 43(1–4):37–55. https://doi.org/10.1016/0377-0273(90)90043-F

Wolff JA, Ellis BS, Ramos FC, Starkel WA, Boroughs S, Olin PH, Bachmann O (2015) Remelting of cumulates as a process for producing chemical zoning in silicic tuffs: a comparison of cool, wet and hot, dry rhyolitic magma systems. Lithos 236–237:275–286. https://doi.org/10.1016/j.lithos.2015.09.002

Worner G, Schmincke HU (1984) Mineralogical and chemical zonation of the Laacher See Tephra Sequence (East Eifel, West-Germany). J Petrol 25(4):805–835

Zollo A, Maercklin N, Vassallo M, Dello Iacono D, Virieux J, Gasparini P (2008) Seismic reflections reveal a massive melt layer feeding Campi Flegrei caldera. Geophys Res Lett 35(12). https://doi.org/10.1029/2008gl034242